Velocity Extension for the Level-set Method and Multiple Eigenvalues in Shape Optimization

Frédéric de Gournay

SIAM J. CONTROL OPTIM.
Vol. 0, No. 0, pp. 000–000

VELOCITY EXTENSION FOR THE LEVEL-SET METHOD AND MULTIPLE EIGENVALUES IN SHAPE OPTIMIZATION*

FRÉDÉRIC DE GOURNAY†

Abstract. In the context of structural optimization by the level-set method, we propose an extension of the velocity of the underlying Hamilton–Jacobi equation. The gradient method is endowed with a Hilbertian structure based on the H^1 Sobolev space. Numerical results for compliance minimization and mechanism design show a strong improvement of the rate of convergence of the level-set method. Another important application is the optimization of multiple eigenvalues.

Key words. multiple eigenvalues, shape optimization, sensitivity analysis, shape derivative, level-set method, regularization

AMS subject classifications. Au please provide

DOI. 10.1137/050624108

1. Introduction.

Optimal design of elastic structures has been widely studied and many different numerical methods are used to solve this problem. Most of the existing methods can be divided into two main classes: topology optimization which optimizes a density of material in each cell and geometric optimization which moves the boundary of the domain.

The most recent topology method, the homogenization method and its variants (power-law method or SIMP method), may be considered quite classical in view of the number of publications (see, e.g., [1], [2], [6], [8], [7], [12]). The homogenization method seems the most promising because it is independent with respect to initialization and because it gives a strong mathematical result of the existence of solution. Sadly this method bears the difficulty of handling quite badly eigenvalue problems where apparitions of so-called fictitious-material modes prevent stable numerical computation. Another problem is that topology methods give optimal shapes that are composite. Penalization methods allow one to project the composite shape on a classical shape (a black-and-white design).

The problem of fictitious modes is naturally solved with the geometric methods where the shape is clearly identified and the void cannot generate fictitious modes.

The major drawback of geometric methods is their dependency with respect to initialization. Even the most recent level-set method ([4], [5], [34]) is very sensitive to initialization although the topology can change. In order to avoid this problem, a method of topology optimization, the bubble method (or topological gradient method [16], [17], [31], [32]), has been recently coupled with geometric optimization (see [3], [11]). Another recent advance in that field has been led by Nazarov and Sokolovski [23], but numerical use of this method is still not done.

We wish here to correct the so-called void problem that arises when using the level-set algorithm. This problem is generated by the weak material approximation that gives rise to a negative velocity for advecting the shape in the void. The void problem slows down the algorithm when the mesh is refined.

*Received by the editors Febuary 9, 2005; accepted for publication (in revised form) October 21, 2005; published electronically DATE.
http://www.siam.org/journals/sicon/x-x/62410.html
†Centre de Mathématiques Appliquées (UMR 7641), Ecole Polytechnique, 91128 Palaiseau, France (degourna@cmapx.polytechnique.fr).

The void problem is presented in section 3, and the chosen solution is presented in section 4. The method mainly consists of applying the Δ^{-1} operator to the velocity which is costless. This method allows one to regularize and to extend and gives a local Hilbertian structure (see the discussion in section 4.2). Numerical results are presented in sections 4.3–4.7; they compare the new method with the previous one and show strong improvements of the level-set algorithm.

The method also has made it possible to deal with the problem of optimizing an eigenvalue when its multiplicity is greater than 1. Theoretical differentiation of the eigenvalue is made in section 5. As can be expected from theory on eigenvalue differentiation, the first eigenvalue is directionally differentiable with respect to shape variation, even when this eigenvalue is multiple. The algorithm that optimizes the first eigenvalue is detailed in section 5.3. It strongly relies on the local Hilbertian structure given by velocity regularization. Indeed, because of this local Hilbertian structure, the differential gives rize to a gradient and therefore to a steepest descent. We show that the choice of the steepest descent is a semidefinite program in low dimension that is easily solved. Some numerical results are presented in section 6.

The method used for optimizing multiple eigenvalues can be extended to other criteria that are not differentiable as the robust compliance criterion in the sense of [13]. The method of velocity regularization presented here is an adaptation of [10], [26], [21]. It is a standard issue in numerical computation.

2. The level-set method in shape optimization.

2.1. Eigenvalue maximization. We set our model problem in linearized elasticity. Let $\Omega \subset \mathbb{R}^d$ ($d = 2$ or 3) be a bounded open set occupied by a linear isotropic elastic material with Hooke's law A_0. Recall that, for any symmetric matrix ξ, A_0 is defined by

$$A_0\xi = 2\mu\xi + \lambda\big(\mathrm{Tr}\xi\big)Id,$$

where μ and λ are the Lamé coefficients of the material. The boundary of Ω is made of two disjoint parts

$$\partial\Omega = \Gamma_N \cup \Gamma_D, \tag{1}$$

with Dirichlet boundary conditions on Γ_D and Neumann boundary conditions on Γ_N. The spectral problem is to find an eigenvalue γ and an eigenvector $u \neq 0$ such that

$$\left\{\begin{array}{rcll} -\mathrm{div}\,(\mathrm{A}\,\mathrm{e}(\mathrm{u})) & = & \gamma\rho u & \text{in } \Omega, \\ u & = & 0 & \text{on } \Gamma_D, \\ \big(A\,e(u)\big)n & = & 0 & \text{on } \Gamma_N, \end{array}\right. \tag{2}$$

where ρ is a scalar field on Ω that represents the material density (typically ρ is equal to 1 on Ω).

It is well known that $\mathrm{Sp}(\Omega)$ the set of eigenvalues is a countable set of positive numbers that tends to infinity. The smallest eigenvalue $\gamma_1(\Omega) = \min \mathrm{Sp}(\Omega)$ can then be defined.

A classical way of improving the rigidity of a structure is to maximize the first eigenfrequency. Thus, a natural objective function to be minimized is

$$\mathcal{L}(\Omega) = -\gamma_1(\Omega) + \eta|\Omega|, \tag{3}$$

where η is a given Lagrange multiplier for a volume constraint. We want to minimize $\mathcal{L}$ with respect to Ω with a constraint that $\Omega \subset D$, where D is a given domain of $\mathbb{R}^d$.

2.2. Classical algorithm. The works [24], [29], or [5] give an extensive explanation of the level-set method. Only the main ideas are to be reviewed in this section.

As described in [4], when the dimension of the eigenspace associated to γ_1 is equal to 1, the above functional $\mathcal{L}(\Omega)$ is differentiable with respect to variation of the domain and the geometrical shape optimization method can be applied. It reads, as follows:

1. **Calculation of the gradient.** Let Ω_k be the domain at iteration k. Assuming that $\gamma_1(\Omega_k)$ is simple, for a given $\theta \in W^{1,\infty}(D;D)$ define

$$(Id+\theta)\circ\Omega_k = \{x+\theta(x) \text{ with } x \in \Omega_k\}.$$

Prove that $\mathcal{L}((Id+\theta)\circ\Omega_k)$ is differentiable with respect to θ at the point $\theta = 0$. The value of $\mathcal{L}'$, the differential at the point 0 is given by

$$\mathcal{L}'(\theta) = \int_{\partial\Omega_k} (\theta\cdot n)(-v+\eta) \tag{4}$$

$$\text{with} \quad \begin{cases} v &= Ae(u)\colon e(u) - \gamma_1 \rho u\cdot u & \text{on} \quad \Gamma_N^k, \\ v &= -Ae(u)\colon e(u) & \text{on} \quad \Gamma_D^k, \end{cases} \tag{5}$$

where u is an eigenvector normalized by $\int_{\Omega_k}\rho u\cdot u = 1$ which is, up to a change of sign, by assumption, unique and where n is the outer normal of Ω_k.

2. **Calculation of a descent direction.** Choose θ_k such that $\mathcal{L}'(\theta_k) < 0$, and let $\Omega_{k+1} = (Id+t\theta_k)\circ\Omega_k$, where t is the step of the gradient method.

The level-set method is a geometrical shape optimization method where the domains Ω_k are represented through functions ϕ_k defined on D in the following way: $x \in \Omega_k \Longleftrightarrow \phi_k(x) < 0$. Such a ϕ_k is said to be "a level set function of Ω_k." Of course for a given domain, the associated level-set functions are not unique.

The changes of topology are then handled in a very simple way (see [5] for extensive explanations of numerical advantages). The method relies on the following lemma.

LEMMA 2.1. *If ϕ_k is a level-set function of Ω_k, define ϕ_{k+1} as*

$$\phi_{k+1} - \phi_k + t(\theta_k\cdot n)|\nabla\phi_k| = 0.$$

Then there exists an $O(t^2)$ such that $\phi_{k+1} + O(t^2)$ is a level-set function for the domains $\Omega_{k+1} = (Id+t\theta_k)\circ\Omega_k$.

Thus, the following scheme for choosing ϕ_{k+1} is the most commonly used:

$$\begin{aligned} \phi(0) &= \phi_k, \\ \frac{\partial\phi}{\partial t} + V^*|\nabla\phi| &= 0, \\ \phi_{k+1} &= \phi(T), \end{aligned} \tag{6}$$

where $T > 0$ is the step of the gradient method and V^* is the descent direction chosen according to the calculation (4) of the differential of J. Defining $V^* = v - \eta$ (v being defined in (4)) is the most commonly used choice; we will call this choice the natural extension method. The goal of this paper is to find a different way of defining V^*.

Remark 2.2. In order to avoid multiple definitions of V^*in the natural extension method, it is supposed that the Dirichlet part of the boundary is fixed and that the v used everywhere in the domain is the one defined for Γ_N.

3. The weak material approximation. The stiffness matrix that corresponds to the linear operator of elasticity is not defined on the nodes that does not belong to Ω, i.e., on $x \in D$ such that $\phi(x) > 0$. In other words, this matrix is not invertible. In order to avoid this problem, the so-called weak material (or ersatz material) approximation consists of fixing Hooke's law A and the material density ρ as

$$\begin{array}{rclcrclcl} A & = & A_0 & \text{and} & \rho & = & 1 & \text{in} & \Omega \\ A & = & \varepsilon A_0 & \text{and} & \rho & = & \varepsilon^\alpha & \text{outside} & \Omega \end{array}$$

with a small parameter ε and $\alpha \geq 1$. The fictitious modes are avoided by setting $\alpha = \infty$. In the continuous case, it has been proven (see [28]) that the eigenvector $\tilde{u}$ calculated by using the ersatz material approximation is equal (at first order in ε) to the desired eigenvector u introduced in (2). In $D \setminus \Omega$ $\tilde{u}$ is the lifting of the Dirichlet condition $\tilde{u} = u$ on $\partial\Omega$ (at first order in ε).

Recalling that the Dirichlet part of the boundary of $\partial\Omega$ has been fixed (see Remark 2.2), $v - \eta = Ae(u) : e(u) - \gamma_1 \rho u \cdot u - \eta$ is defined everywhere on D, and the natural extension method consists of defining $V^* = Ae(u) : e(u) - \gamma_1 \rho u \cdot u - \eta$ on every cell.

This nevertheless raises a problem: since u is everywhere of order ε^0, then $Ae(u) : e(u)$ is of order ε outside Ω which means that the velocity extension is almost equal to $-\eta$ outside the domain and makes it very difficult for the shape to increase its volume. Even if the descent step T is increased in order to speed up the method, the parts of the shape where there is a need to decrease the volume will move faster than the parts of the shape where there is a demand on increasing the volume.

In numerical result, it can be seen that between each computation of the eigenvalue, the level-set method cannot move $\partial\Omega$ of more than one cell away from the original boundary when it wants to improve the volume. This leads to a drastically increasing computational time with mesh-refinement.

This remark is true, of course, for every objective function and not only for the minimization of the first eigenvalue.

4. Velocity regularization by the Hilbertian method.

4.1. Definition of the Hilbertian method. We will suppose that the domain Ω has enough regularity so that $v(\cdot, \cdot)$ defined in (4) belongs to $H^{-1/2}(\partial\Omega)$. Even if the optimal domain may possibly be irregular, physical and numerical intelligence tells that throughout optimization $v(\cdot, \cdot)$ has the required regularity but mathematical proof of this fact is still lacking. Let us first define a scalar product.

DEFINITION 4.1. *For $a \in \mathbb{R}^{*+}$, define the following scalar product on $H^1(D)$:*

$$(u, w)_{H^1} = \int_D a \nabla u \cdot \nabla w + uw$$

with the associated norm $\| \cdot \|_{H^1}$.

The velocity V^* in the Hamilton–Jacobi equation (6) is chosen as the unique solution to

$$\int_{\partial\Omega} V^*(-v + \eta) = \min_{\substack{V \in H^1(D) \\ \|V\|_{H^1} = 1}} \int_{\partial\Omega} V(-v + \eta), \tag{7}$$

where v is the differential defined in proposition (4) and Ω is the actual working domain.

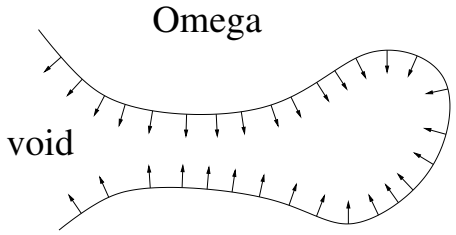

FIG. 1. *Two merging parts of the boundary leads to a nonregular vector field as seen as a distribution on D.*

4.2. Advantages of the method.

Scalar versus vector. We choose to extend the normal velocity which is a scalar field, i.e., if θ is the vector field that advects the domain, its normal velocity is equal to $\theta \cdot n$ on the boundary of the domain. Seen as a distribution over D, the normal velocity is more regular than the vector velocity. A good example is when two parts of the boundary want to merge: $\theta \cdot n$ is positive on the two parts and θ changes orientation. This situation gets worse at the next step of the algorithm (see Figure 1). That is why the normal velocity is extended and not the vector velocity.

How to compute V^*. The problem of finding V^* is not difficult. Let $\bar{V}$ be the unique solution to

$$(\bar{V}, X)_{H^1} = \int_{\partial\Omega} X(-v+\eta) \quad \forall X \in H^1(D),$$

where $(\cdot,\cdot)_{H^1}$ is the scalar product of Definition 4.1. Then $V^* = -\frac{\bar{V}}{\|\bar{V}\|_{H^1}}$ and the inversion of the matrix that corresponds to the scalar product $(\cdot,\cdot)_{H^1}$ has to be done only once in the optimization process.

Extension, regularization, and Hilbertian structure. Three different goals are sought in the Hilbertian extension of the velocity.

First, the formula for the differential of $\mathcal{L}$ gives a velocity that makes sense only on the boundary of the domain, and the Hamilton–Jacobi equation (6) needs a speed defined everywhere on the domain or else the algorithm cannot move the boundary of more than one cell during optimization. This is the extension issue.

Secondly, the velocity is regularized by being diffused with the scalar product defined in Definition 4.1. This is the regularization issue. It is expected to increase the accuracy of the algorithm and is a standard issue in optimization problems (see, e.g., [26], [10], [21]).

Thirdly, the problem is endowed with a Hilbertian structure, and we work with gradient-type methods. This issue will be developed later in section 5.

Hilbertian extension versus other extensions. The most natural way to extend the velocity outside $\partial\Omega$ would have been to extend $v - \eta$ according to the normal of $\partial\Omega$ by a front-propagating-type method such as the fast-marching method described in [25]. This method does not endow the space with a Hilbertian structure. Neither does it regularize the velocity.

V^* is indeed an extension. Because the scalar product diffuses the source term, the velocity is now defined everywhere on D, and the typical problem of null velocity in the void that raises with the natural extension method is now cured.

V^* is indeed a regularization. V^*, the speed used in the Hilbertian extension method, is more regular than $v - \eta$, the speed used in the natural extension method as can be seen in the following formal derivation.

FIG. 2. *Boundary conditions for a two-dimensional (2d) cantilever (the black zone is heavier and not subject to optimization).*

If v belongs to an $H^s(D)$, then $X \mapsto \int_{\partial\Omega} X(-v+\eta)$ is a linear form on $H^{-s+1/2}(D)$, and V^* belongs to an $H^{s+3/2}(D)$ by elliptic regularity on the very smooth domain D. Indeed V^* is obtained by operating an inverse Laplacian on the distribution (on D) $X \mapsto \int_{\partial\Omega} X(-v+\eta)$ and so gains two derivatives.

Consistency of the extension. This algorithm could be seen as a gradient-type algorithm if there were a vector field $\theta^* \in W^{1,\infty}(D;D)$ such that $\theta^* \cdot n = V^*$ on $\partial\Omega$. Two hypotheses would then be needed: a certain regularity on V^* and a certain regularity of the domain Ω itself.

In order to ensure regularity of V^*, a scalar product on H^p, $p \geq 1$, could have been used instead of a scalar product on H^1. In this case, formally, V^* would have $2p - 1/2$ more derivatives in L^2 than v. But numerical computation of V^* may be quite difficult. Indeed, the computation of the matrix of the scalar product of H^p needs finite elements that are chosen according to p.

The extension parameters. The coefficient a characterizes the diffusion of $v-\eta$ in the sense that setting it small compared to 1 will lead to a solution V^* which is pointwise almost equal to $v-\eta$ on $\partial\Omega$ or equal to 0 outside $\partial\Omega$. It must be set small enough so that a big value of $|v-\eta|$ on one part of the boundary does not interfere too much with the values of $v-\eta$ on the other parts of the boundary. But it must be set big enough in order to diffuse the value of $v-\eta$ outside the boundary of Ω.

4.3. Numerical example: Eigenvalues of a cantilever. We study a medium-cantilever problem. The working domain is a 2×1 rectangle, with zero displacement condition on the left side and a small square region at the middle of the right side (see Figure 2) which is 500 times heavier and not subject to optimization. This heavier mass allows one to avoid trivial shapes (see Figure 3). The Young modulus of the material is set to 1, the Poisson ratio ν to 0.3, and the Lagrange multiplier to 7×10^{-2}. In the void, the ersatz material has a Young modulus set to 10^{-5} and a density ρ set to 0. The mesh is refined alternatively in each direction by a factor of 2, and the number of transport iterations is adequately increased at each mesh refinement (see the table below).

Explanation of Table 1. Table 1 lists, for different meshes, the number of transport iterations used for each optimization step in the Hamilton–Jacobi equation, the average computed time used per iteration step of the gradient method, and the global computing time. The number of transport iterations is shown for the Hilbertian method only. The number of transport iterations for the natural method is 16 times the number of transport iterations of the Hilbertian method. This explains why the average time per iteration of the gradient algorithm is bigger for the natural method than for the Hilbertian. The last column is the global computing time for obtaining

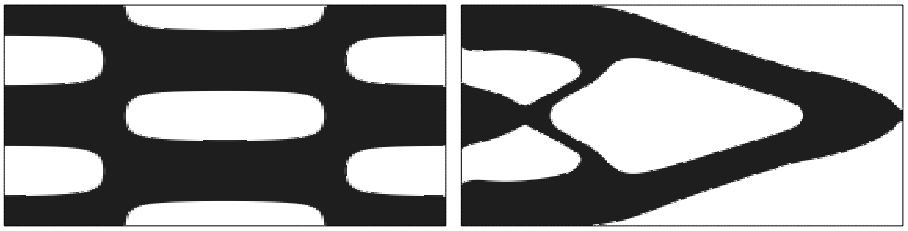

FIG. 3. *Initialization and optimal shape for the first eigenvalue of a cantilever.*

TABLE 1
Data of the numerical test.

Mesh	N^o of transport	Time per iteration Hilbertian / natural	Global time Hilbertian / natural
81×41	16	1.46 / 1.62	30.68 / 50.13
161×81	32	9.35 / 11.37	233.87 / 330.01
321×161	64	72.17 / 94.91	2237.2 / 2657.63
41×41	14	0.74 / 0.84	13.26 / 22.6
81×81	28	4.46 / 6.19	120.62 / 136.1
161×161	56	38.50 / 46.61	1116.57 / 1771.44

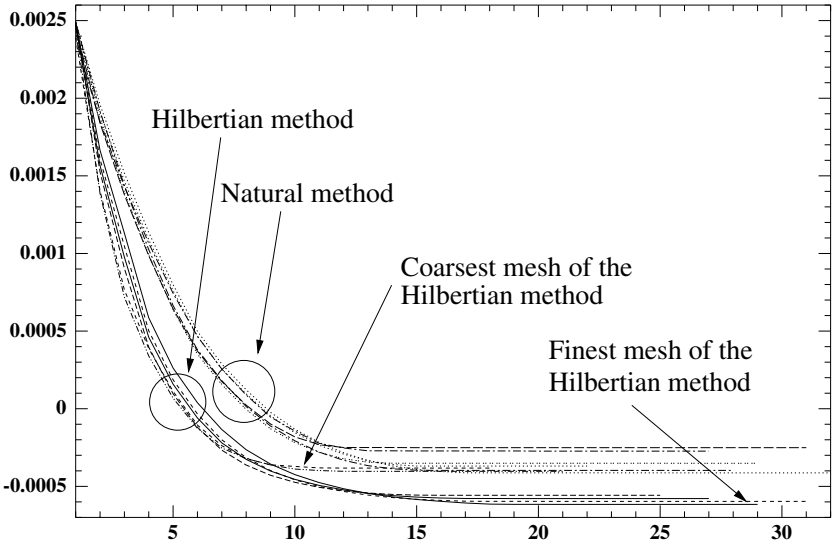

FIG. 4. *Mesh-refinement influence on the velocity for the natural extension (left) and the Hilbertian extension (right).*

the optimal shape. The Hilbertian method takes the same amount of time as the natural method to obtain the optimal shape but only because it is more accurate. As can be seen in Figure 4, the convergence curves of the Hilbertian method are indeed better than the convergence curves of the natural method. Time is given in seconds.

Explanation of Figure 4. There is two sets of curves in Figure 4. The better ones are obtained with the Hilbertian method. It appears that the more the mesh is refined, the better the optimal shape is, even if, when the mesh is refined, the

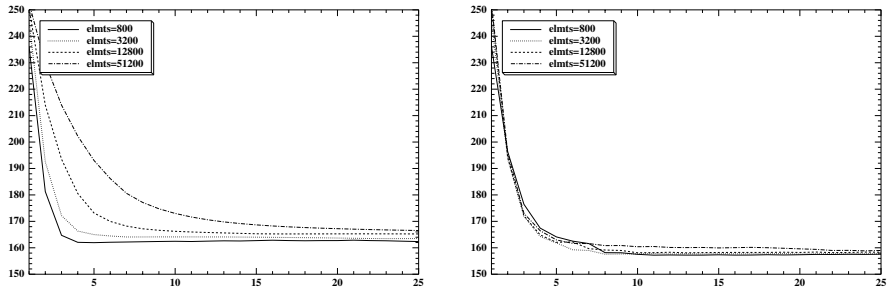

FIG. 5. *Mesh-refinement influence on the natural extension (left) and the Hilbertian extension (right).*

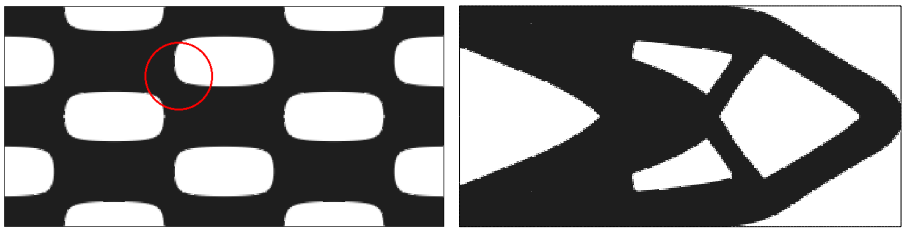

FIG. 6. *Initialization and optimal shape of the cantilever.*

decreasing of the smallest eigenvalue leads to an increase of the criterion. This is easily explained by a better accuracy on the optimal shape itself.

Remark 4.2. In order to prove mesh-consistency of the algorithm and to have comparable curves in Figure 4, the optimal shape has to be the same when the mesh is changed. Thus those examples are chosen so that there is no possibility for the algorithm to create thin structures when the mesh is refined. This explains why there are a very few holes in the initialization. It is well known that the level-set algorithm can produce more complicated structures.

4.4. Numerical example: The compliance of the cantilever. We performed our new velocity extension method on the well-known cantilever problem which is fixed on the left wall and supports a unit vertical point load in the middle of the right wall. The compliance is here optimized. The working domain size is 2×1. The Young modulus is set to 1, and the Poisson ratio to 0.3. The Lagrange multiplier is set to $\eta = 100$.

Optimization is performed for several finer meshes, and the number of transport iterations is multiplied by 2 as each square of the mesh is cut into 4 squares. For the finest mesh (321×161) that corresponds to 51200 elements; the number of transport iterations is equal to 128 for the natural extension and to 16 for the Hilbertian. As a result, the Hilbertian extension is really quicker.

Mesh-refinement influence. The curves in Figure 5 show that the Hilbertian method is less sensitive to mesh-refinement than the natural method. Because there are parts of the boundary that have to increase the volume (one of them is circled in Figure 6) and the natural extension method has problems to improve these parts as was said in section 3, the natural extension method is sensitive to mesh-refinement. In Figure 4 there was no such demand on improving the volume and the mesh-independence of the Hilbertian method was less obvious.

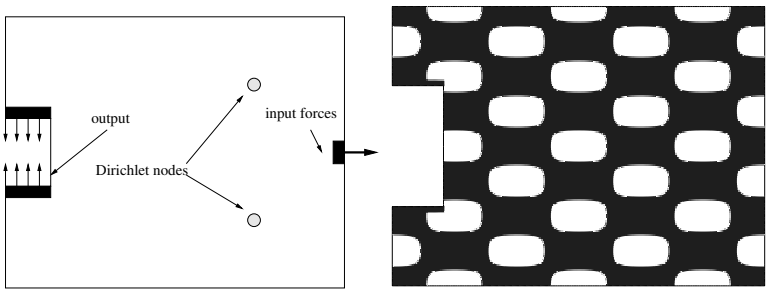

FIG. 7. *The definition of the* 2*d gripping mechanism and its initialization.*

4.5. Numerical example: A two-dimensional (2d) gripping-mechanism. On a 1.2×3.2 rectangle meshed with 241×641 nodes, we give a numerical example for minimizing the least square of a prescribed displacement. This example was given by the Comissariat à l'Energie Atomique for the design of a grip (see [9]). The objective function is

$$\mathcal{J}_{lse}(\Omega) = \int_{\Omega} k(x)|u(x) - u_0(x)|^2, \tag{8}$$

where u is the displacement obtained by a given set of forces, u_0 is a prescribed given displacement, and k is a scalar field that characterizes the zone of interest.

The ponderation k is equal to 10 on the left black box in Figure 7 (left), is equal to 1 on the right black box, and is equal to 0 elsewhere. The prescribed displacement u_0 is equal to $(0, \pm 1)$ on the left black box, and $(0, 0)$ on the right box. Enforcing u to be close to 0 where the force is input allows one to ensure the stiffness and the connectivity of the structure. These black boxes are not subject to optimization.

A force of modulus 1 N is applied in the x-direction on the middle of the left, and a uniform pressure which represents a total force of modulus 5×10^{-2} N is applied between the jaws of the mechanism in order to force the mechanism to hold objects. The prescribed displacement is located on the black box on the left as shown in Figure 7. The Young modulus is set to 1, the Poisson ratio to 0.3, and there is a small Lagrange multiplier of a volume constraint of value 0.05. This Lagrange multiplier helps remove parts of the boundary that are useless.

This is a typical problem where an adjoint is needed. For some reason that is not completely understood, the ratio of the weak material (the factor ε in section 3) cannot be set too low (typically it must be at least 1 percent of the strong material) or the algorithm will not work. One of the explanations that may be given is the tendency of the shape to create hinges. The algorithm then concentrates on the hinges only, ignoring the rest of the shape, and it is believed it is then stuck in a local minimum. If the ratio of the weak material is high, hinges are less efficient and the previous problem is avoided.

Optimization must then be made in two steps. First the shape is optimized with a ratio of the weak material equal to 1 percent. The optimal shape is then reoptimized with a smaller ratio (10^{-5} in this numerical case). In the second optimization procedure, the displacement and the adjoint state are calculated with a more accurate precision which leads to a better precision of the shape-derivative.

In Figure 8 (left), it may seem that the Hilbertian method is less efficient than the natural method. This is explained by the lack of precision in the computation

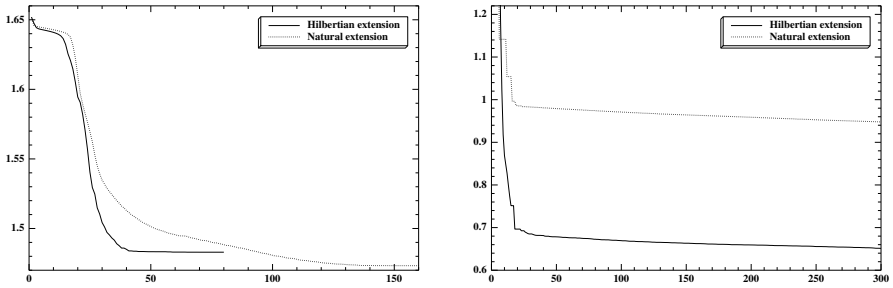

FIG. 8. *Evolution of the objective function for the first step (left) with a ratio for the weak material equal to* 0.01 *and the second step with a ratio of* 10^{-5} *(right).*

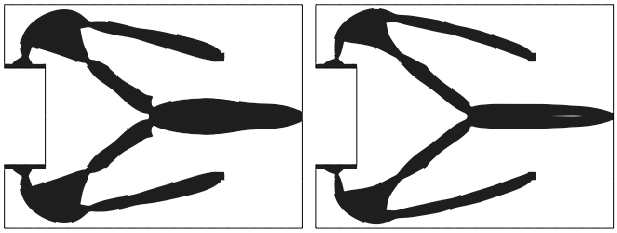

FIG. 9. *Optimal shape for the Hilbertian method (left) and the natural method (right) at the end of the first step of optimization.*

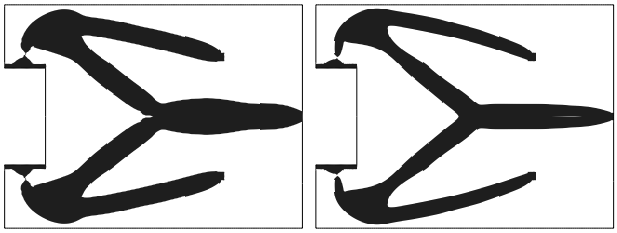

FIG. 10. *Optimal shape for the Hilbertian method (left) and the natural method (right) at the end of the second step of optimization.*

of the shape-derivative in the first step of the algorithm. But it is also explained by the lack of precision of the computation of the criterion during the first step of the algorithm. Indeed when the two shapes of Figure 9 (obtained with $\varepsilon = 10^{-2}$) are computed using $\varepsilon = 10^{-5}$, the Hilbertian shape is the better one.

Remark 4.3. The optimal shape for the natural extension method has less volume than the one for the Hilbertian extension (see Figures 10 and 11) it is a numerical validation of the problem raised in section 3.

4.6. Numerical example: More 2d mechanisms. We briefly present here some more 2d mechanisms: namely, a negative Poisson modulus cell (Figures 12 to 14) and a force inverter (Figures 15 to 17). These examples are standards of shape optimization problems, and their description can be found in [8]. In order to ensure stiffness of the structures, a small pressure load is applied where the displacement is optimized (on the right black box of Figure 15 for the force inverter and at the

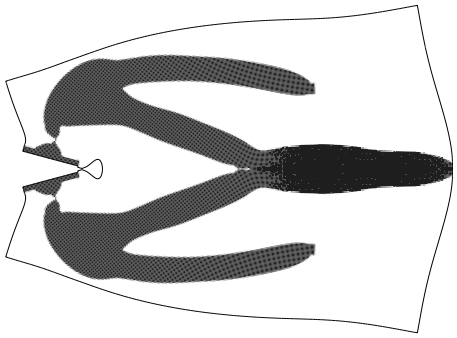

FIG. 11. *Optimal shape displacement.*

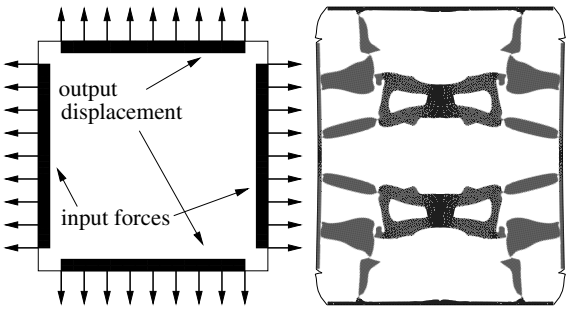

FIG. 12. *The Negative Poisson modulus problem and its deformed solution.*

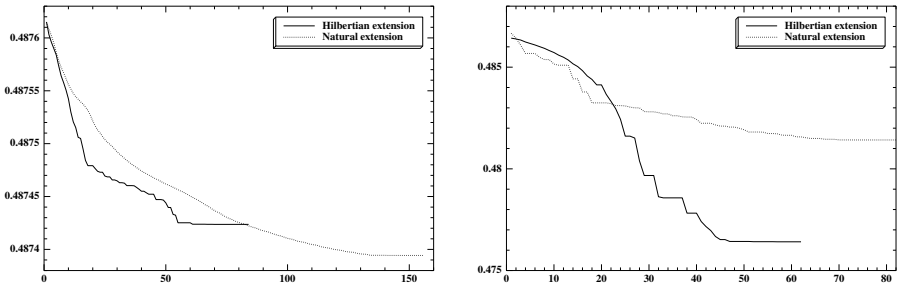

FIG. 13. *Negative Poisson modulus's evolution of the objective function at the first step (left) with a ratio for the weak material equal to* 0.01 *and the second step with a ratio of* 10^{-5} *(right).*

top and bottom of Figure 12 for the negative Poisson modulus mechanism). At the location of the input forces (left black box for the force inverter or the left and right walls for the negative Poisson modulus mechanism), the displacement is enforced to be close to zero in order to ensure connectivity of the shapes. Optimization is made in two steps like the 2d grip of section 4.5, and the behavior of the Hilbertian extension with respect to the natural extension is comparable.

4.7. Numerical example: A three-dimensional (3d) gripping mechanism. The objective function is defined by (8) in section 4.5. The working domain is a $3 \times 2 \times 6$ rectangle. A uniform pressure load is applied on the plane $x = 3$, and the

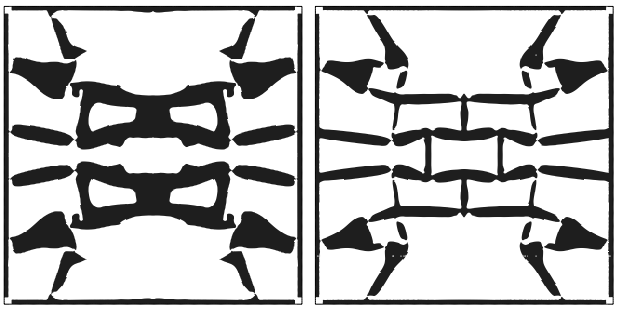

FIG. 14. *Negative Poisson modulus's optimal shape for the Hilbertian method (left) and the natural method (right) at the end of optimization.*

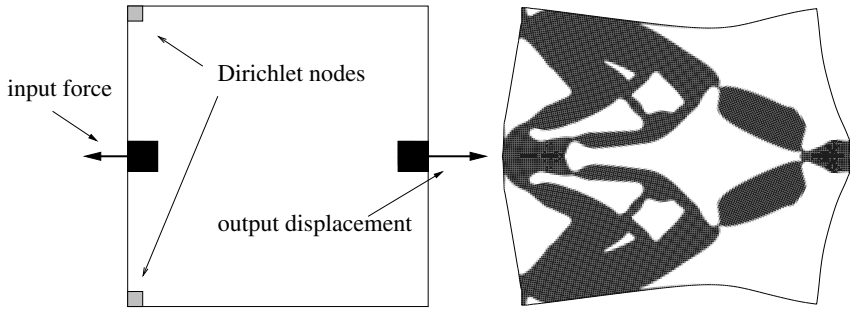

FIG. 15. *The force inverter problem and its deformed solution.*

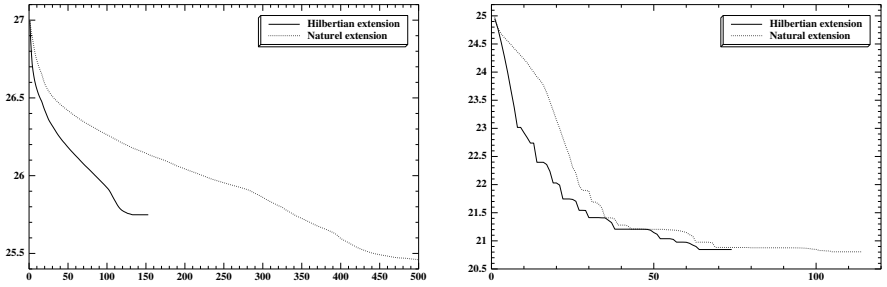

FIG. 16. *Force inverter's evolution of the objective function for the first step (left) with a ratio for the weak material equal to* 0.01 *and the second step with a ratio of* 10^{-5} *(right).*

prescribed displacement is localized on a box at the opposite side (see Figure 18 where a cross-section at $y = 0$ is shown). A uniform pressure load (of order 60 percent of the one on the plane $x = 3$) is also imposed between the jaws of the mechanism so that this mechanism is designed to hold and grip. The Poisson ratio is 0.3, and the Young modulus is 1. The Lagrange multiplier is set to 3, and the mesh used is $31 \times 21 \times 61$. The ratio of the weak material is set to 10^{-5}. There is no need here to perform the 2-step optimization of section 4.5. The reason why things seems to be simpler in 3d is that the changes of topology and the hinges are not of the same nature as in 2d; consequently, it is believed that throughout the process of optimization, the objective function is more regular in 3d.

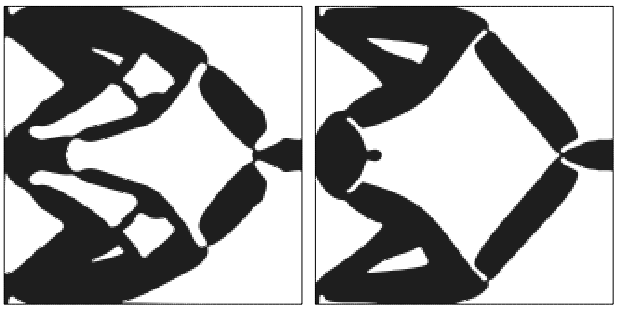

FIG. 17. *Force inverter's optimal shape for the Hilbertian method (left) and the natural method (right) at the end of optimization.*

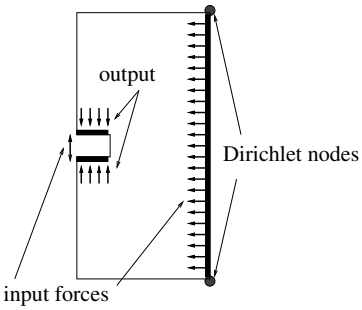

FIG. 18. *The problem of the* 3*d gripping mechanism.*

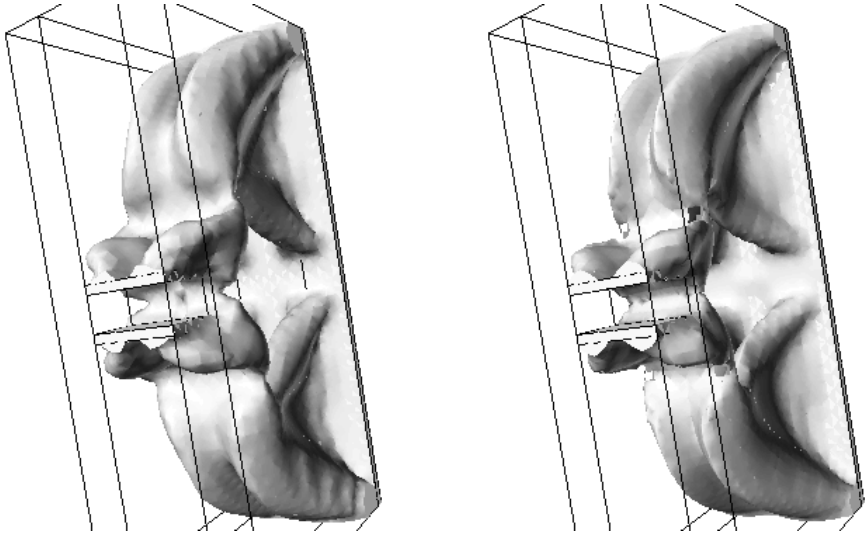

FIG. 19. *Optimal shape for the Hilbertian method (left) and the natural method (right) (isovalue* 0 *of the level-set is shown).*

5. Optimizing multiple eigenvalues. The development above for optimizing the first eigenvalue stands only when this eigenvalue is of multiplicity equal to 1. When this is not the case, there is no more differentiability of the first eigenvalue with respect

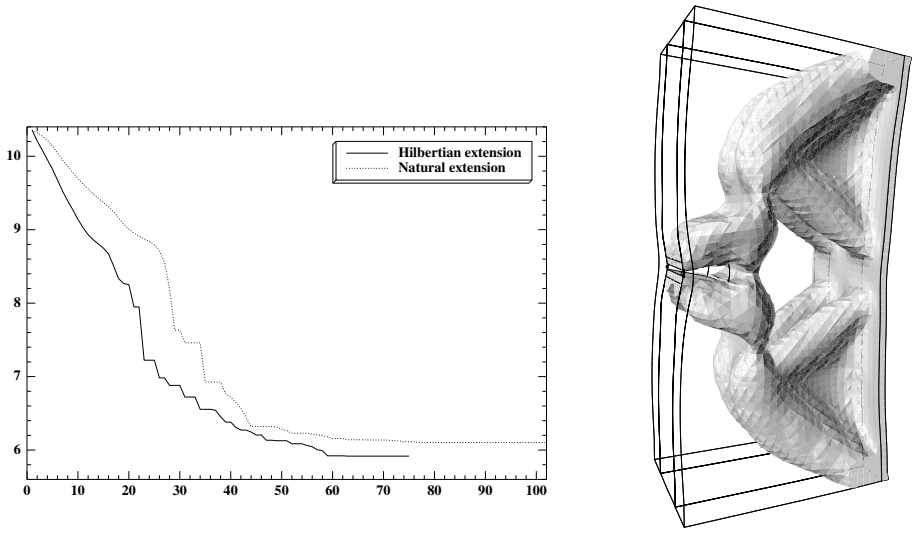

FIG. 20. *Objective function (left) and displacement of the Hilbertian shape (right) (density of material* ≥ 0.3 *is shown).*

to θ, and the above method cannot be applied. Nevertheless it has been proven that $\mathcal{L}$ is directionally differentiable. The velocity extension which endows the space with a Hilbertian structure allows one to find a direction of descent. The algorithm used is now a subgradient-type algorithm. The goal of this section is two-fold:

1. Calculate $\mathcal{L}'(\theta) : W^{1,\infty}(D;D) \to \mathbb{R}$ the nonlinear collection of directional derivative of $\mathcal{L}$. Show that according to Hadamard's structure theorem $\mathcal{L}'(\theta)$ depends only on the value of $\theta \cdot n$ on $\partial\Omega$. Let us denote $j(\theta \cdot n) = \mathcal{L}'(\theta)$.

2. Compute V^* such that $j(V^*) = \min_{\|V\|=1} j(V)$, and advance the domain according to V^*. It is in the computation of V^* that the Hilbertian structure is compulsorily needed.

5.1. A general theorem about eigenvalue differentiation. Differentiating eigenvalues when they are multiple is nowadays quite standard. Two different approaches exist: the one of [19] for the foundations or [27] and [20], or the one of [15] or [18] using the subgradient theory of Clarke [14]. We shall only state their result here.

DEFINITION 5.1. *Define* Ω_0 *as the actual working domain.*

$\diamond$ *Let* $\alpha > 0$, $\beta_1 > 0$ *be constants and* $\mathbb{L}$ *be the space of linear unbounded auto-adjoint operators from* $L^2(\Omega_0) \to L^2(\Omega_0)$ *such that*

$$\forall L \in \mathbb{L}, \quad \forall u \in H^1_D(\Omega_0) \quad \beta_1 \|u\|^2_{H^1_D(\Omega_0)} \geq (Lu,u)_{L^2} \geq \alpha \|u\|^2_{H^1_D(\Omega_0)},$$

i.e., $\mathbb{L}$ *is made of operators "uniformly" coercive with constant* α *and uniformly continuous with constant* β_1

$\diamond$ *Let* $\beta_2 > 0$ *be a constant and* $\mathbb{M}$ *be the space of continuous linear auto-adjoint operators from* $L^2(\Omega_0) \to L^2(\Omega_0)$ *uniformly continuous with constant* β_2*, i.e.,*

$$\forall M \in \mathbb{M}, \quad \forall u \in L^2(\Omega_0) \quad \beta_2 \|u\|^2_{L^2(\Omega_0)} \geq (Mu,u)_{L^2}.$$

$\diamond$ *Define the norm in those two spaces as follows: If* $N \in \mathbb{L}$ *or* $N \in \mathbb{M}$*, then*

$$\|N\| = \max_{u \in H^1_D} \frac{(Nu,u)_{L^2}}{\|u\|^2_{H^1_D}},$$

i.e., we endow $\mathbb{M}$ *with the natural norm of* $\mathbb{L}$*.*

$\diamond$ *Let* $U \subset W^{1,\infty}(D;D) \to \mathbb{L} \times \mathbb{M}$ *be a Fréchet differentiable mapping* $\theta \mapsto (L(\theta), M(\theta))$ *with respect to the norm just defined. Define* $L'(\theta_0)$ *(resp.* $M'(\theta_0)$*) the differential of* $L(\theta)$ *(resp.* $M(\theta)$*) with respect to* θ *at the point* $\theta = 0$ *applied to* θ_0*.*

THEOREM 5.2. *Define* $\gamma_1(\theta)$ *the smallest eigenvalue of the generalized eigenproblem* $L(\theta)u = \gamma M(\theta)u$ *and* E_θ *its eigenspace,* $E_\theta = Ker(L(\theta) - \gamma_1 M(\theta))$*. Then, for all* $\theta_0 \in W^{1,\infty}(D;D)$*,* $\gamma_1(\theta)$ *is directionally differentiable at the point* $\theta = 0$ *in the direction* θ_0 *and the value of the directional derivative is*

$$\gamma_1'(\theta_0) = \min_{\substack{u \in E_0 \\ (M(0)u,u)=1}} \big(L'(\theta_0)u, u\big) - \gamma_1(0)\big(M'(\theta_0)u, u\big).$$

5.2. Calculus of the directional derivative of $\mathcal{L}$. We want to apply the general Theorem 5.2 in the shape sensitivity setting. We want to derivate $\tilde{\mathcal{L}}(\theta)$ defined as below.

DEFINITION 5.3.

$\diamond$ *Let* $T = Id + \theta$ *and* $\Omega_\theta = T \circ \Omega_0$*.*

$\diamond$ *Let* $\tilde{M}(\theta)$ *and* $\tilde{L}(\theta)$ *be defined as for all* u, v *in* $H^1_D(\Omega_\theta)$*,*

$$(\tilde{M}(\theta)u, v) = \int_{\Omega_\theta} \rho u \cdot v$$
$$(\tilde{L}(\theta)u, v) = \int_{\Omega_\theta} Ae(u) : e(v).$$

$\diamond$ *Let* $\tilde{\gamma}_1(\theta)$ *be the smallest eigenvalue associated to the problem*

$$\tilde{L}(\theta)u = \tilde{\gamma}_1(\theta)\tilde{M}(\theta)u.$$

$\diamond$ *Let* $\tilde{\mathcal{L}}(\theta) = -\tilde{\gamma}_1(\theta) + \eta|\Omega_\theta|$*.*

The $\tilde{\mathcal{L}}(\theta)$ (resp. $\tilde{\gamma}_1(\theta)$) just defined corresponds to what has been denoted $\mathcal{L}(\Omega_\theta)$ (resp. $\gamma_1(\Omega_\theta)$) in section 2.1.

Theorem 5.2 cannot be applied to $\tilde{\gamma}_1(\theta)$ because the spaces where the operators $\tilde{L}(\theta)$ and $\tilde{M}(\theta)$ are defined changes with θ. That is why we consider the following definition.

DEFINITION 5.4.

$\diamond$ *Let* $M(\theta) \in \mathbb{M}$ *and* $L(\theta) \in \mathbb{L}$ *be defined as*

$$(M(\theta)u, v) = (\tilde{M}(\theta)u \circ T^{-1}, v \circ T^{-1})$$
$$(L(\theta)u, v) = (\tilde{L}(\theta)u \circ T^{-1}, v \circ T^{-1}).$$

$\diamond$ *Let* $\bar{\gamma}(\theta)$ *be the smallest eigenvalue associated to the problem*

$$L(\theta)u = \bar{\gamma}(\theta)M(\theta)u.$$

We shall work with those operators instead of the classical one. They are defined on a domain independent of θ so that the first eigenvalue can be derivated in the sense

of Theorem 5.2. First it must be proven that the introduced eigenvalue $\bar{\gamma}$ is the same as γ_1 the first eigenvalue of the elasticity problem.

LEMMA 5.5.

$\diamond$ *$L(\theta)$ and $M(\theta)$ indeed belongs to $\mathbb{L}$ and $\mathbb{M}$.*

$\diamond$ *$\bar{\gamma}(\theta)$ and $\tilde{\gamma}_1(\theta)$ coincide, where $\tilde{\gamma}_1$ is defined in Definition 5.3.*

Proof of Lemma 5.5.

$\diamond$ Let us first prove that $\tilde{\gamma}_1(\theta) = \bar{\gamma}(\theta)$. Using $u \in H^1(\Omega_\theta) \Longleftrightarrow v = u \circ T^{-1} \in H^1(\Omega_0)$, we have

$$\begin{aligned}\tilde{\gamma}_1(\theta)^{-1} &= \max_{u \in H^1(\Omega_\theta)} \frac{\big(\tilde{M}(\theta)u, u\big)}{\big(\tilde{L}(\theta)u, u\big)} = \max_{u \in H^1(\Omega_\theta)} \frac{\big(M(\theta)u \circ T, u \circ T\big)}{\big(L(\theta)u \circ T, u \circ T\big)} \\ &= \max_{v \in H^1(\Omega_0)} \frac{\big(M(\theta)v, v\big)}{\big(L(\theta)v, v\big)} = \bar{\gamma}(\theta)^{-1}.\end{aligned}$$

$\diamond$ Let us now prove that $L(\theta)$ belongs to $\mathbb{L}$. The fact that $L(\theta)$ is coercive and bounded with respect to the $H^1_D(\Omega_0)$ norm comes from the fact that $\tilde{L}(\theta)$ is coercive and bounded in the $H^1_D(\Omega_\theta)$ norm. We have to show that these constants of coercivity and boundedness are uniform in θ. Let's introduce the tensor A which has the symmetries of the elasticity:

$$A^{ijkl} = A^{jikl} = A^{ijlk} = A^{klij}$$

such that $A^{ijkl}(\partial_j u^i)(\partial_l v^k) = Ae(u) : e(v)$. We use the standard tool of shape sensitivity, namely a change of variable:

$$\begin{aligned}(L(\theta)u, v) &= \int_{\Omega_\theta} A^{ijkl} \partial_j (u \circ T^{-1})^i \partial_l (v \circ T^{-1})^k \\ &= \int_{\Omega_0} |\det \nabla T| A^{ijkl} (\partial_s u^i) \left(\partial_j (T^{-1})^s\right) (\partial_m v^k) \left(\partial_l (T^{-1})^m\right) \qquad (9) \\ &= \int_{\Omega_0} l(\theta)^{iskm} (\partial_s u^i)(\partial_m v^k)\end{aligned}$$

with

$$l(\theta)^{iskm} = A^{iskm} + (\partial_l \theta^l) A^{iskm} - A^{ijkm}(\partial_j \theta^s) - A^{iskl}(\partial_l \theta^m) + o(\|\theta\|_{W^{1,\infty}}).$$

Given α and β the coercivity and continuity constant of $L(0)$, there exist $\eta > 0$ such that (s.t.) for every θ with $\|\theta\|_{W^{1,\infty}} < \eta$, we have

$$\forall u \in H^1_D(\Omega_0) \quad 2\beta_0 \|u\|^2_{H^1_D(\Omega_0)} \geq (L(\theta)u, u)_{L^2} \geq \frac{\alpha_0}{2} \|u\|^2_{H^1_D(\Omega_0)}.$$

We then verify the hypothesis of Definition 5.1 with $\alpha_1 = \alpha/2$, $\beta_1 = 2\beta$, and $U = \{\theta \text{ s.t. } \|\theta\|_{W^{1,\infty}} < \eta\}$. An analog development stands for M. ∎

We can now apply Theorem 5.2 to $\bar{\gamma}(\theta) = \tilde{\gamma}_1(\theta)$ and end with the following result.

THEOREM 5.6. *Recalling Definition* 5.3, *$\tilde{\mathcal{L}}(\theta) = -\tilde{\gamma}_1(\theta) + \eta|\Omega_\theta|$ is directionally differentiable with respect to θ, and its directionally derivative at $\theta = 0$ in the direction θ_0 is given by*

$$\mathcal{L}'(\theta_0) = \max_{\substack{u \in E_0 \\ \int_{\Omega_0} \rho u \cdot u = 1}} \int_{\partial\Omega_0} (\theta_0 \cdot n) \left(-v(u,u) + \eta\right),$$

where $v(\cdot,\cdot)$ is a bilinear functional defined by

$$\begin{aligned} v(u,w) &= Ae(u)\colon e(w) - \gamma_1\rho(\Omega_0)u\cdot w \quad \text{on } \Gamma_N,\\ v(u,w) &= -Ae(u)\colon e(w) \quad \text{on } \Gamma_D, \end{aligned}$$

and where E_0 is the first eigenspace associated to $\gamma_1(\Omega_0) = \tilde{\gamma}(0)$ the smallest eigenvalue for $\theta = 0$.

One can of course verify that the formula when the dimension of the eigenspace is greater than 1 is the same as the formula when the dimension is equal to one.

Proof of Theorem 5.6. We apply Theorem 5.2 to $\tilde{\gamma}_1(\theta) = \bar{\gamma}(\theta)$ in order to calculate $\mathcal{L}'(\theta_0)$. The calculus above for L (and the same for M) shows that

$$\begin{aligned} (L'(\theta)u,v) = & \int_{\Omega_0} \left((\partial_l\theta^l)A^{iskm} - A^{ijkm}(\partial_j\theta^s) - A^{iskl}(\partial_l\theta^m)\right)(\partial_s u^i)(\partial_m v^k)\\ = & \int_{\Omega_0} A^{iskm}(\partial_l\theta^l)(\partial_s u^i)(\partial_m v^k) - A^{iskm}(\partial_s\theta^l)(\partial_l u^i)(\partial_m v^k)\\ & -A^{iskm}(\partial_m\theta^l)(\partial_s u^i)(\partial_l v^k),\\ (M'(\theta)u,v) = & \int_{\Omega_0} (\partial_l\theta^l)\rho u^i v^i. \end{aligned}$$

Applying Theorem 5.2 gives

$$\begin{aligned} \mathcal{L}' = \max_{\substack{u\in E_0\\ \int_{\Omega_0}\rho u\cdot u=1}} & -\int_{\Omega_0} A^{iskm}(\partial_l\theta^l)(\partial_s u^i)(\partial_m v^k) + A^{iskm}(\partial_s\theta^l)(\partial_l u^i)(\partial_m v^k)\\ & +\int_{\Omega_0} A^{iskm}(\partial_m\theta^l)(\partial_s u^i)(\partial_l v^k) + (\partial_l\theta^l)\rho u^i v^i + \eta(\partial_l\theta^l). \end{aligned} \tag{10}$$

We perform an integration by part on θ; the term in $\int_{\Omega_0}$ is equal to

$$\theta^l A^{iskm}\left[\partial_l(\partial_s u^i\partial_m u^k) - \partial_s(\partial_l u^i\partial_m u^k) - \partial_m(\partial_s u^i\partial_l u^k)\right] - \theta^l\gamma_1\rho\partial_l(u^i u^i). \tag{11}$$

Some algebra used in coordination with $\gamma_1\rho u = -\mathrm{divAe(u)}$ allows us to conclude that this term is equal to 0. The remaining term is then equal to

$$\begin{aligned} \mathcal{L}'(\theta) = & \max\int_{\partial\Omega_0} (\theta\cdot n)[-A^{iskm}(\partial_s u^i)(\partial_m u^k) + \gamma_1\rho u\cdot u + \eta]\\ & +\int_{\partial\Omega_0} A^{iskm}\theta^l n^m(\partial_s u^i)(\partial_l u^k) + A^{iskm}\theta^l n^s(\partial_l u^i)(\partial_m u^k). \end{aligned} \tag{12}$$

On the Neumann part of the boundary we use $Ae(u)\cdot n = 0$ and the definition of C to conclude that

$$A^{iskm}(\partial_s u^i)n^m = 0 = A^{iskm}(\partial_m u^k)n^s.$$

On the Dirichlet part of the boundary we use $u = 0$ so that $\nabla u = \frac{\partial u}{\partial n}\otimes n$ to conclude that

$$(\theta\cdot n)(\partial_m u^k) = \theta^l n^m(\partial_l u^k) \text{ and } (\theta\cdot n)(\partial_s u^i) = \theta^l n^s(\partial_l u^i)$$

so that

$$\mathcal{L}'(\theta) = \max\int_{\partial\Omega_0} (\theta\cdot n)[-Ae(u)\colon e(u) + \gamma_1 u\cdot u + \eta] + 2\int_{\Gamma_D}(\theta\cdot n)Ae(u)\colon e(u). \qquad \square$$

Remark 5.7 (*Assumed regularity of* Ω_0). We need regularity on the domain Ω_0 in two occurrences. The first one is when we perform a change of variable ((9) in the demonstration of Lemma 5.5), and the second one is when we perform an integration by part ((11) in the demonstration of Theorem 5.6).

The change of variable is compulsory in order to prove the derivability. It is sufficient to suppose Ω_0 Lipschitz in order to be able to perform it.

The integration by part is used only in order to express the directional derivative (10) as an integral over $\partial\Omega_0$ (see (12)). Performing this integration by part is asking a lot of regularity on Ω_0 because the eigenvector u must be regular enough, i.e., $u \in H^1(\partial\Omega_0)$. But this integration by part is not needed if the only goal is to prove the directional derivability.

5.3. Calculating V^*. The goal of this subsection is to calculate V^* the minimizer to

$$\min_{\|V\|=1} \max_{\substack{u\in E_0 \\ \int_{\Omega_0} u\cdot u=1}} \int_{\partial\Omega_0} V\left(-v(u,u)+\eta\right), \tag{13}$$

where $v(\cdot,\cdot)$ is defined in Theorem 5.6. We will prove in this section that this is a semidefinite programming (SDP) problem in low dimension that is easily solved. The use of SDP for eigenvalue optimization is classical; the goal of this section is to show that solving this SDP problem is a very easy task thanks to the Hilbertian structure endowed by the velocity regularization. A good introduction to SDP is [33] and the references therein. Only some basic facts about SDP problems have been recalled here.

Definition 5.8.

$\diamond$ *Let Y be an unknown vector. Give Y_0 a vector and $E(Y)$ a matrix whose coefficients depend linearly on Y. Let ≥ 0 stand for "symmetric positive." An SDP problem is of the form*

$$\min_{E(Y)\geq 0} Y^T Y_0.$$

$\diamond$ *SDP problems are efficiently solvable by duality methods. In order to ensure that there is no gap of duality, a sufficient condition is to find Y_1 a strictly primal feasible point, i.e., such that $E(Y_1) > 0$ (definite positive).*

We now need to introduce the semidefinite programming problem we will work on.

Definition 5.9. *Recall Definition* 4.1 *of the scalar product $(\cdot,\cdot)_{H^1}$.*
$\diamond$ *Define $(e_i)_{i=1,\dots,d}$ an orthonormal basis of E_0 for the scalar product*

$$(u,w) = \int_{\Omega_0} \rho u\cdot v.$$

$\diamond$ *Define $(a_{ij})_{i,j=1,\dots,d}$ and c as*

$$(a_{ij},X)_{H^1} = \int_{\partial\Omega_0} -Xv(e_i,e_j) \quad \textit{and} \quad (c,X)_{H^1} = \int_{\partial\Omega_0} X\eta.$$

$\diamond$ *Define h_k an orthonormalized basis of $Span(a_{ij},c)_{i,j}$ for the scalar product $(,)_{H^1}$. Let m be the dimension of this space, and let $(a_{ij}^k)_{k=1,\dots,m}$ (resp. $(c^k)_{k=1,\dots,m}$) be the coordinates of a_{ij} (resp. c) on the basis $(h_k)_{k=1,\dots,m}$.*

$\diamond$ *For any* $X = (X_1, \dots, X_m)$ *and* $(z, w) \in \mathbb{R}^2$, *let* $Y = [X, w, z]$.
$\diamond$ *Let* $A(X)$ *be the* $d \times d$ *matrix* $A(X)_{ij} = a_{ij}^k X_k$, *let* $C(X) = c^k X_k$, *and let*

$$D(Y) = \begin{bmatrix} -A(X) + zId & 0 \\ 0 & -C(X) - z + w \end{bmatrix}, \quad E(Y) = \begin{bmatrix} D(Y) & 0 & 0 \\ 0 & Id & X \\ 0 & X^T & 1 \end{bmatrix}.$$

The coefficients of E *depends linearly on* $Y = [X, w, z]$.
$\diamond$ *Let* $Y^* = [X^*, w^*, z^*]$ *be the solution of the following SDP problem:*

$$\min_{E(Y) \geq 0} w \tag{14}$$

THEOREM 5.10. V^*, *the minimizer of the problem* (13), *is given by*

$$V^* = \sum_{k=1}^{m} V_k h_k,$$

where the vector $X^* = [V_1, \dots, V_k]$ *is defined as a solution of the semidefinite problem* (14).
$\diamond$ *The problem* $\min_{E(Y) \geq 0} w$ *is strictly feasible; SDP programming can be applied.*
$\diamond$ V^* *(or equivalently* X^**) is attained.*

Proof. We transform the problem (13) into (14) by using the fact that $v(\cdot, \cdot)$ is bilinear (see Theorem 5.6 for the definition of v)

$$\begin{aligned} &\min_{\|V\|_{H^1}=1} \max_{\substack{u \in E_0 \\ \int_{\Omega_0} \rho u \cdot u = 1}} \int_{\partial\Omega_0} V[-v(u,u) + \eta] \\ &= \min_{\|V\|_{H^1}=1} \max_{\sum_{i=1}^d \lambda_i^2 = 1} \int_{\partial\Omega_0} V[-\lambda_i \lambda_j v(e_i, e_j) + \eta] \\ &= \min_{\|V\|_{H^1}=1} \max_{\sum_{i=1}^d \lambda_i^2 = 1} \lambda_i \lambda_j (V, a_{ij})_{H^1} + (V, c)_{H^1} \\ &= \min_{\|V\|_{H^1}=1} \max_{\sum_{i=1}^d \lambda_i^2 = 1} (V, h_k)_{H^1} (\lambda_i \lambda_j a_{ij}^k + c^k) \end{aligned}$$

so that V^* is a minimizer of (13) if and only if $X_k^* = (V^*, h_k)_{H^1}$ are minimizers of the following problem:

$$\min_{\sum X_k^2 \leq 1} \max_{\sum_{i=1}^d \lambda_i^2 = 1} \lambda_i \lambda_j a_{ij}^k X_k + c^k X_k. \tag{15}$$

$\diamond$ Showing that (15) is equivalent to (14) is a standard issue of SDP: The condition $E([X, w, z]) \geq 0$ is equivalent to $(X, X) \leq 1$ and $D([X, w, z]) \geq 0$. The condition $D([X, w, z]) \geq 0$ is equivalent to $zId \geq A(X)$ and $w \geq z + C(X)$. So

$$E([X, w, z]) \geq 0 \Longleftrightarrow \sum_k X_k^2 \leq 1 \text{ and } w \geq z + X_k c^k \text{ and } z \geq \max_{\sum_{i=1}^d \lambda_i^2 = 1} \lambda_i \lambda_j a_{ij}^k X_k$$

so that minimizing w with the above condition is equivalent to finding X in the problem (15).

$\diamond$ Choosing $X = 0$, $z > 0$, and $w > z$ gives a $[X, w, z]$ for which $F([X, w, z]) > 0$. The problem is then strictly feasible, an extended Slater's condition holds, and the

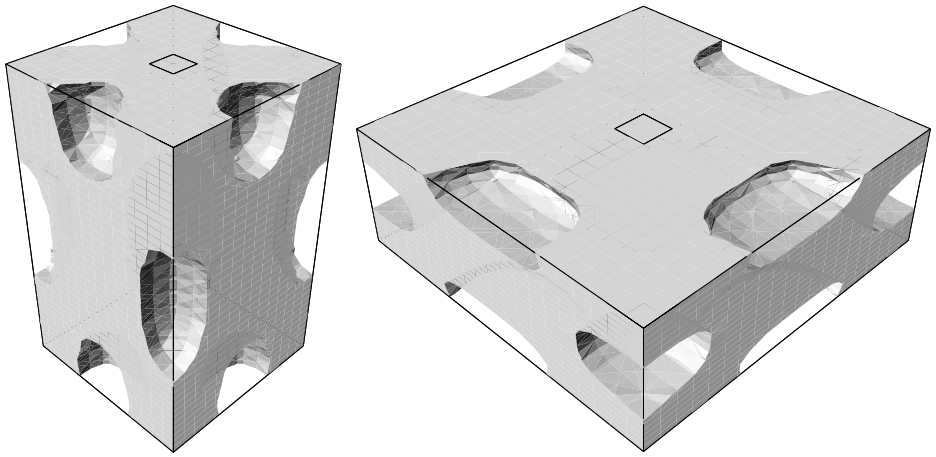

FIG. 21. *Initialization for the narrow domain (left) and for the big domain (right).*

duality problem (in terms of semidefinite duality) has the same extremal value.
$\diamond$ The condition $\sum_k X_k^2 \leq 1$ ensures that X is bounded and that every minimizing sequence converges up to a subsequence. The maximum is indeed attained. $\square$

Remark 5.11. The SDP problem is not difficult to solve. Recall that d is the dimension of the first eigenspace, then $[X, w, z]$ is of dimension lower or equal to $\frac{d(d+1)}{2} + 3$ and the matrix E is a $\frac{d(d+3)}{2} + 3$ square matrix.

6. Numerical results.

6.1. The 3d eigenvalue of a beam. We naturally set our problem in 3d with symmetries, where we are sure to obtain a multiplicity of the first eigenvalue greater than 1. The first example which will be called the "big domain" problem is a $3 \times 3 \times 1$ rectangle discretized with a $21 \times 21 \times 23$ mesh. A zero displacement boundary condition is imposed on the plane $z = 0$, and four cells on the middle of the plane $z = 1$ are not subject to optimization and are 50 times heavier (see Figure 21). Since the domain is symmetric, the shapes are expected to keep a first eigenvalue of dimension at least 2 along the iterations (see Figure 22). The Young's modulus is set to 1 and the Poisson ratio to 0.3. In the void, the density ρ is set to 0 and the parameter ε is equal to 10^{-5}. The second problem is the same as the first except that the rectangle is of dimension $0.6 \times 0.6 \times 1$ (discretized by a $15 \times 15 \times 43$ mesh) with a mass tip that is 200 times heavier. The second problem will be called in this section the "narrow domain" problem.

Discussion about the big domain problem. The Lagrange multiplier being set to 5.3×10^{-8}, Figure 23 is a display of the evolution of the three smallest eigenvalues. There is one eigenvalue that is always (except on iterations 22 to 28) of multiplicity two and one which is of multiplicity one. The eigenvalue of multiplicity one corresponds to an eigenvector which is localized on the heavy cells and that interferes in the optimization process. The panel on the left-hand side of Figure 23 shows the evolution of the eigenvalues. On each iteration, the value of d the dimension of the subspace of the first eigenvalue is shown. The expected behavior of the algorithm can be verified.

Discussion about the narrow domain problem. As can be seen in Figure 25 (left), the global evolution of the algorithm is as follows: First reinforce the structure

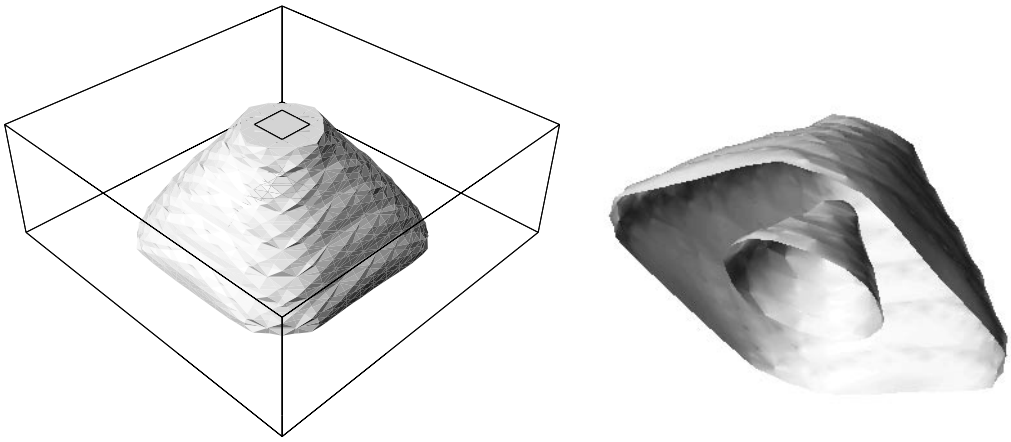

FIG. 22. *The optimal shape for the first eigenvalue in a big domain (left) and its boundary (right).*

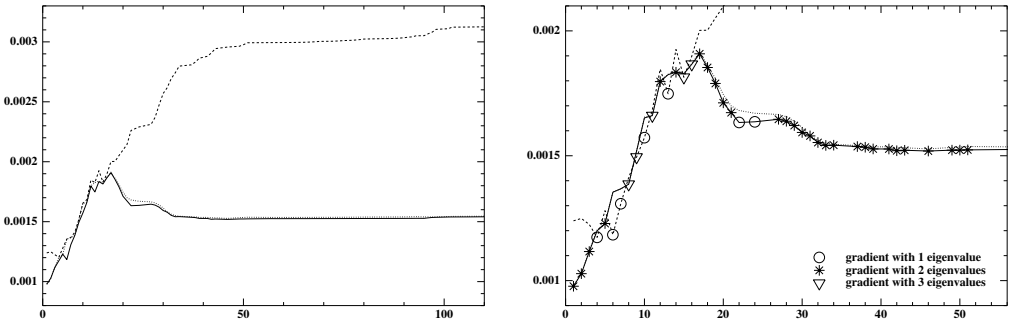

FIG. 23. *Evolution of the three smallest eigenvalues (left) and an interpretation (right) for the big domain.*

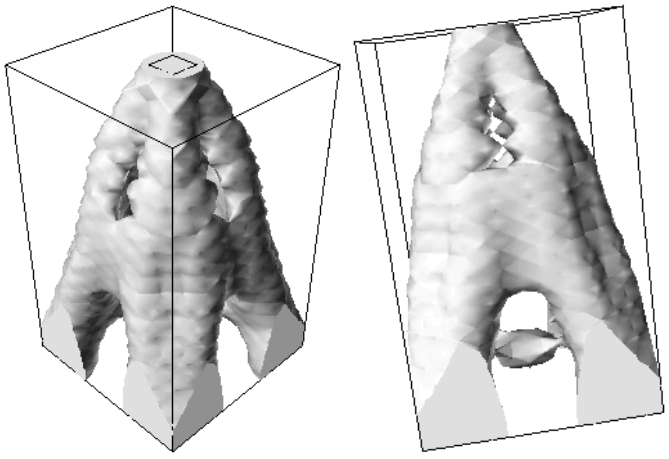

FIG. 24. *The optimal shape for the first eigenvalue in a narrow domain (isovalue* 0.2 *of the density is drawn).*

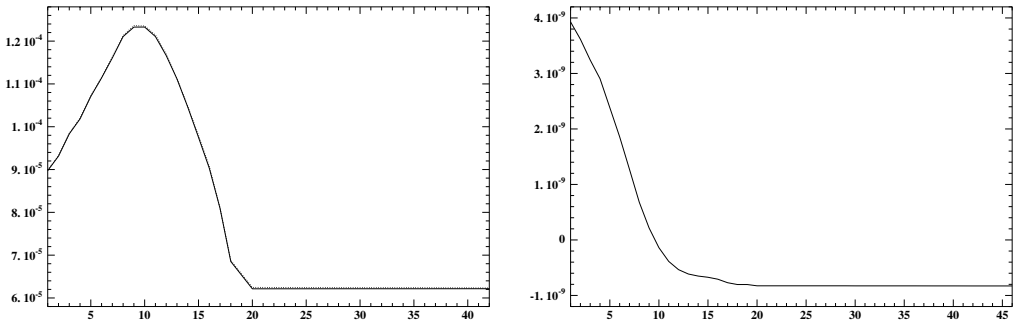

FIG. 25. *Evolution of the two smallest eigenvalues (left) and the objective function (right) for the narrow domain.*

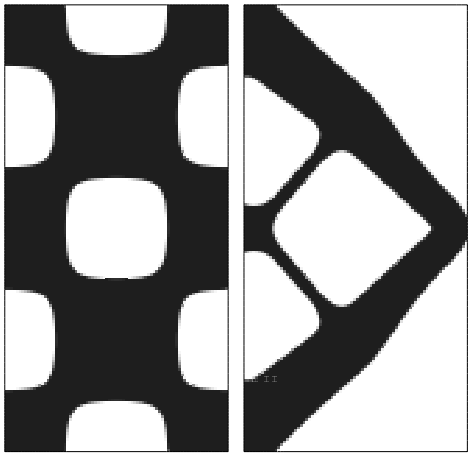

FIG. 26. *Initialization and optimal shape for the first eigenvalue of a short cantilever.*

so that the first eigenvalue raises, and then optimize the weight of the structure. The Lagrange multiplier is set to 10^{-8} for this example.

Discussion about the symmetries. Neither of the two problems give rise to radially symmetrical shapes. For the narrow-domain problem it can be easily understood by the fact that the shape is constrained into a box. For the big-domain problem one can advance an explanation based on a mesh-effect. But it is known that there exist symmetric problems whose solutions do not respect the symmetries. We still do not know if the optimal shape is or is not radially symmetric for this problem.

6.2. The short cantilever. We run our algorithm on a vibrating cantilever that is the same test case as the one of section 4.3 except that the working domain is of size 1×2 discretized with a regular 80×160 mesh. The other parameters that have changed are the Lagrange multiplier which is set to 0.3 and the heavier mass which has a density 80 times heavier. This test case was introduced in [4] where the authors pointed out the appearance of multiple eigenvalues. It is not the exact same test because when the test of [4] has been run, the improvement of the multiple eigenvalue method is not as obvious as in the test presented here.

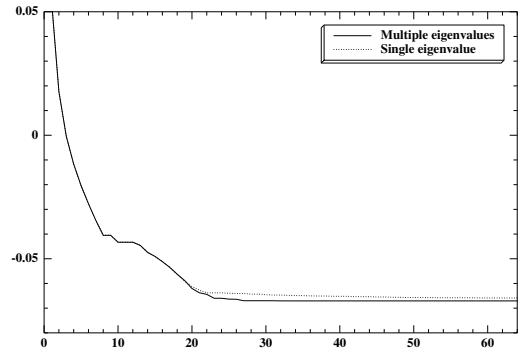

FIG. 27. *Evolution of the objective function for the two different methods.*

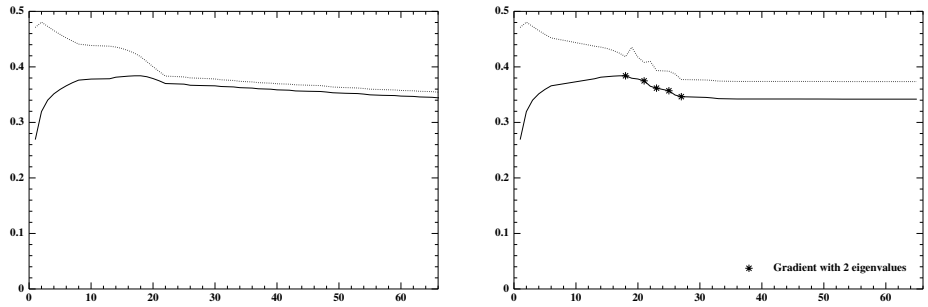

FIG. 28. *Evolution of the two smallest eigenvalues for the single eigenvalue optimization (left) and for the multiple eigenvalue optimization (right).*

The test is run with the standard single eigenvalue optimization (only one eigenvalue is taken into account during optimization) and the multiple eigenvalue optimization processes (see Figure 26). Figure 27 shows the evolution of the objectives functions for the two different processes.

At iteration n, the algorithm considers an eigenvalue to be of multiplicity d if and only if the relative differences $\gamma_d/\gamma_1 - 1 \leq \epsilon_0 < \gamma_{d+1}/\gamma_1 - 1$, where ε_0 is a user-defined criterion. If the shape computed at iteration $n+1$ is not better than the shape computed at iteration n and if the eigenvalue at iteration n is multiple, then the parameter ε_0 is decreased. The parameter ε_0 is set to 10 percent at the beginning of the optimization process. This explains the behavior of the algorithm in Figure 28 (right).

It can be seen in Figure 28 (left) that when the first eigenvalue is considered to be always of multiplicity one, the two first eigenvalues have a tendency to merge and the algorithm cannot improve the shape. If we follow the branches of eigenvalues according to the modes, we would see that the smallest eigenvalue does not correspond to the same modes during optimization, i.e., the algorithm optimizes one mode at iteration n and another one at iteration $n+1$. This is standard of optimization with respect to a maximum of a function when the maximum is multiple and it is well known to slow down the algorithm.

7. Conclusion. The velocity-regularization method presented here improves the speed and accuracy of the level-set method and extends it to new problems. Thanks to the Hilbertian method, three issues can be dealt with: the extension, the regularization, and the endowment of a Hilbertian structure (see the discussion in section 4.2).

The extension issue (i.e., extending everywhere a velocity which is only defined on the boundary) is related only to the speed of the algorithm. The 2d compliant cantilever of section 4.4 which shows the mesh-independence of the Hilbertian method is a good example of the improvements this new method brings to the level-set algorithm.

The regularization issue is about dealing with more regular velocities. It is indeed an improvement as can be seen in the mechanism examples because it allows one to improve the accuracy of the optimal shape. It allows one to also improve the speed of the algorithm by diffusing the peaks of the velocity in the vicinity of the peak. The only test for which velocity regularization is not as efficient in terms of accuracy as the natural extension is the first step of the optimization procedure of the 2d mechanism of section 4.5 (see Figure 8 (left)). This can be explained by the fact that the adjoint is not computed with a precision that is accurate enough when the ratio of the weak material is too high. Sadly for 2d tests which need the computation of an adjoint, it still seems compulsory to perform the 2-steps optimization procedure. It was seen in section 4.7 that this trick is not needed in 3d.

Because the velocity regularization endows the problem with a Hilbertian structure, it allows one to apply the level-set method of optimization for several problems that are not differentiable but whose directional derivative exists. The computation of the descent direction relies on an SDP problem. The transformation of the steepest descent algorithm into an SDP problem can be made because the directional derivative of the problem is a maximum of quadratic functions over a sphere. This is the case for the eigenvalue problem, for the robust compliance problem, and for the buckling load problem which are all based on the generalized eigenvalues problem. The investigation of the two latest problems and application of the Hilbertian method to those issues is in progress.

Acknowledgments. I deeply thank Grégoire Allaire for his advise on this work, for his useful and always pertinent comments and suggestions, and François Jouve for his programming skills and useful critics. Every figure was obtained by using François Jouve's personal software.

REFERENCES

[1] G. Allaire, *Shape Optimization by the Homogenization Method*, Springer-Verlag, New York, 2001.
[2] G. Allaire, E. Bonnetier, G. Francfort, and F. Jouve, *Shape optimization by the homogenization method*, Nümer. Math., 76 (1997), pp. 27–68.
[3] G. Allaire, F. de Gournay, F. Jouve, and A.-M. Toader, *Structural optimization using topological and shape sensitivity via a level set method*, Control Cybernet., to appear.
[4] G. Allaire and F. Jouve, *A level-set method for vibrations and multiple loads in structural optimization*, Comput. Methods Appl. Mech. Engrg., (2005).
[5] G. Allaire, F. Jouve, and A.-M. Toader, *Structural optimization using sensitivity analysis and a level-set method*, J. Comput. Phys., 194 (2004), pp. 363–393.
[6] M. Bendsoe, *Methods for Optimization of Structural Topology, Shape and Material*, Springer-Verlag, New York, 1995.
[7] M. Bendsoe and N. Kikuchi, *Generating optimal topologies in structural design using a homogenization method*, Comput. Methods Appl. Mech. Eng., 71 (1988), pp. 197–227.

[8] M. Bendsoe and O. Sigmund, *Topology Optimization. Theory, Methods, and Applications*, Springer-Verlag, New York, 2003.
[9] P. Bernardoni, *Outils et méthode de conception de structure mécaniques à déformations et actionnements répartis*, Ph.D. thesis, Université Paris VI, 2004.
[10] M. Burger, *A framework for the construction of level set methods for shape optimization and reconstruction*, Interfaces Free Bound., 5 (2003), pp. 301–329.
[11] M. Burger, B. Hackl, and W. Ring, *Incorporating topological derivatives into level set methods*, J. Comput. Phys., 194 (2004), pp. 344–362.
[12] A. Cherkaev, *Variational Methods for Structural Optimization*, Springer-Verlag, New York, 2000.
[13] A. Cherkaev and E. Cherkaeva, *Principal compliance and robust optimal design*, J. Elasticity, 72 (2003), pp. 71–98.
[14] F. H. Clarke, *Optimization and Nonsmooth Analysis*, Classics Appl. Math. 5, SIAM, Philadelphia, 1990.
[15] S. J. Cox, *The generalized gradient at a multiple eigenvalue*, J. Funct. Anal., (1995).
[16] H. Eschenauer and A. Schumacher, *Bubble method for topology and shape optimization of structures*, Struct. Optim., 8 (1994), pp. 42–51.
[17] S. Garreau, P. Guillaume, and M. Masmoudi, *The topological asymptotic for pde systems: the elasticity case*, SIAM J. Control Optim., 39 (2001), pp. 1756–1778.
[18] F. de Gournay, *Optimisation de formes par la méthode des lignes de niveaux*, Ph.D. thesis, Ecole Polytechnique, 2005.
[19] T. Kato, *Perturbation Theory for Linear Operators*, Springer-Verlag, New York, 1976.
[20] G.-W. Litvinov, *Optimization in Elliptic Problems with Applications to Mechanics of Deformable Bodies and Fluid Mechanics*, Oper. Theory Adv. Appl. 119, Birkhäuser, Basel, 2000.
[21] B. Mohammadi and O. Pironneau, *Applied Shape Optimization for Fluids*, Clarendon Press, Oxford, 2001.
[22] F. Murat and S. Simon, *Etudes de Problèmes d'Optimal Design*, in Lecture Notes in Comput. Sci. 41, Springer-Verlag, Berlin, 1976, pp. 54–62.
[23] S. A. Nazarov and Y. Sokolovski, *The topological derivative of the dirichlet integral under the formation of a thin bridge*, Siberian Math. J., 45 (2004), pp. 341–355.
[24] S. Osher and F. Santosa, *Level-set methods for optimization problems involving geometry and constraints: Frequencies of a two-density inhomogeneous drum*, J. Comput. Phys., 171 (2001), pp. 272–288.
[25] S. Osher and J.-A. Sethian, *Front propagating with curvature dependent speed: Algorithms based on Hamilton-Jacobi formulations*, J. Comput. Phys., 78 (1988), pp. 12–49.
[26] B. Protas, T.-R. Bewley, and G. Hagen, *A computationnal framework for the regularization of adjoint analysis in multiscale pde systems*, J. Comput. Phys., 195 (2004), pp. 49–89.
[27] B. Rousselet and D. Chenais, *Continuité et différentiabilité d'élements propres: Application à l'optimisation de structures*, Appl. Math. Optim., 22 (1990), pp. 27–59.
[28] J. Sanchez-Hubert and E. Sanchez-Palencia, *Vibration and Coupling of Continuous Systems. Asymptotic Methods*, Springer-Verlag, Berlin, 1989.
[29] J.-A. Sethian and A. Wiegmann, *Structural boundary design via level-set and immersed interface methods.*, J. Comput. Phys., 163 (2000), pp. 489–528.
[30] J. Simon, *Differentiation with respect to the domain in boundary value problems.*, Numer. Funct. Anal. Optim., 2 (1980), pp. 649–687.
[31] J. Sokolowski and J.-P. Zolesio, *Introduction to Shape Optimization: Shape Sensitivity Analysis*, Springer Ser. Comput. Math. 16, Springer-Verlag, New York, 1992.
[32] J. Sokolowski and A. Zochowski, *Topological derivatives of shape functionals for elasticity systems*, Mech. Structures Mach., 29 (2001), pp. 331–349.
[33] L. Vandenberghe and S. Boyd, *Semidefinite programming*, SIAM Rev., 38 (1996), pp. 49–95.
[34] M.-Y. Wang, X. Wang, and D. Guo, *A level-set method for structural topology optimization*, Comput. Methods Appl. Mech. Engrg., 192 (2003), pp. 227–246.